Available online at www.sciencedirect.com
ScienceDirect
Journal of Solid State Chemistry 181 (2008) 334–339
JOURNAL OF SOLID STATE CHEMISTRY
www.elsevier.com/locate/jssc

Crystal chemistry of Co-doped $Zn_7Sb_2O_{12}$

Richard Harrington*, Gabrielle C. Miles, Anthony R. West

Department of Engineering Materials, The University of Sheffield, Mappin Street, Sheffield S1 3JD, UK

Received 1 August 2007; received in revised form 8 November 2007; accepted 27 November 2007
Available online 14 January 2008

Abstract

$Zn_7Sb_2O_{12}$ forms a full range of Co-containing α solid solutions, $Zn_{7-x}Co_xSb_2O_{12}$, with an inverse-spinel structure at high temperature. At low temperatures for $x<2$, the solid solutions transform into the low temperature β-polymorph. For $x=0$, the $\beta\rightarrow\alpha$ transition occurs at $1225\pm25\,^{\circ}C$; the transition temperature decreases with increasing x. At high x and low temperatures, α solid solutions are formed but are non-stoichiometric; the (Zn + Co):Sb ratio is >7:2 and the compensation for the deficiency in Sb is attributed to the partial oxidation of Co^{2+} to Co^{3+}. From Rietveld refinements using ND data, Co occupies both octahedral and tetrahedral sites at intermediate values of x, but an octahedral preference attributed to crystal field stabilisation, causes the lattice parameter plot to deviate negatively from the Vegard's law. Sub-solidus compatibility relations in the ternary system ZnO–Sb_2O_5–CoO have been determined at 1100 °C for the compositions containing ⩽50% Sb_2O_5.

Keywords: Varistors; Transition metal oxides; $Zn_7Sb_2O_{12}$; Phase diagrams; Vegard's law

1. Introduction

$Zn_7Sb_2O_{12}$ [1–3] is a well-known secondary phase in ZnO-based varistor ceramics [4], which usually contain transition metal ion dopants including Ni, Co and Cr [5–8]. Undoped $Zn_7Sb_2O_{12}$ is polymorphic; the transition from the low-temperature β-polymorph to the high-temperature α-polymorph occurs at $1225\pm25\,^{\circ}C$ [9]. The α-polymorph has an inverse-spinel structure; the β-polymorph adopts a more complex orthorhombic structure [10].

The effect of α-$Zn_7Sb_2O_{12}$ in ZnO-based varistor ceramics appears to be to reduce the average grain size during the processing of the final ceramic; this leads to an increased number of Schottky barriers associated with grain–grain contacts and results in an improved varistor action with a higher α coefficient. This coefficient α is associated with non-linearity in the current (I)–voltage (V) characteristics, given by the formula

$$I=\left(\frac{V}{C}\right)^{\alpha},$$

where C is a constant [11,12].

Doping $Zn_7Sb_2O_{12}$ with Co appears to stabilise the high-temperature α phase to lower temperatures. Some β-polymorph was observed in the composition $Zn_{6.3}Co_{0.7}Sb_2O_{12}$ [13]; compositions with higher Co content gave the α-polymorph, exclusively. A complete solid solution between α-$Zn_7Sb_2O_{12}$ and $Co_7Sb_2O_{12}$ was reported with a linear decrease in the lattice parameter with x for $Zn_{7-x}Co_xSb_2O_{12}$ [14], from $a=8.6047$ Å for $x=0$ [9] to $a=8.5371$ Å for $x=7$ [15].

It was found that high temperatures were required to form single-phase Co-doped $Zn_7Sb_2O_{12}$; the temperature needed increased with the increasing Co concentration. Even when synthesised by citrate gel methods, which have the advantage of giving atomic scale mixing of the starting materials, samples $x=5$–7 heated at 1000 °C for 1 h contained trirutile $Zn_{1-z}Co_zSb_2O_6$ as a second phase [16,17].

As with $Zn_7Sb_2O_{12}$ [9], $Co_7Sb_2O_{12}$ exists as an inverse spinel and can be written as $(Co_3)_{tet}[Co_4Sb_2]_{oct}O_{12}$ [15]. At intermediate values of x, Zn and Co ions have a choice between the octahedral (16d) and the tetrahedral (8a) sites. Ilic et al. [14], using XRD data, suggested that Co occupies the octahedral site exclusively up to $x=4$, after which substitution on the tetrahedral site takes place. It was,

*Corresponding author. Fax: +44 144 2225943.
E-mail address: Richard.Harrington81@googlemail.com (R. Harrington).

0022-4596/$ - see front matter © 2007 Elsevier Inc. All rights reserved.
doi:10.1016/j.jssc.2007.11.025

however, conceded that due to the insensitivity of XRD to elements with a similar atomic number, some mixing could occur around $x = 4$. Investigations into other spinel systems containing Zn and Co showed a degree of mixing of these cations between octahedral and tetrahedral sites, with Co having a preference for octahedral coordination [18].

The purpose of the present study was to investigate further the location of cations in α-$Zn_{7-x}Co_xSb_2O_{12}$, determine the phase diagram of Co-doped $Zn_7Sb_2O_{12}$ and the sub-solidus phase-compatibility relations in the ternary system ZnO–Sb_2O_5–CoO.

2. Experimental

Reagents used were ZnO (99.99%, Aldrich), Sb_2O_3 (99.99%, Aldrich) and $Co(CH_3COO)_2 \cdot 4H_2O$ (98 + %, Aldrich). The ZnO was dried at 600 °C and Sb_2O_3 at 200 °C; the cobalt acetate was used undried; thermogravimetric analysis confirmed that its water content was close to 4. Starting materials were weighed out to give 0.5–3 g totals. These were mixed in an agate mortar and pestle with acetone, dried and fired in Pt foil boats. Samples were heated slowly from room temperature to 500 °C to drive off water and decompose the acetate. The samples were then removed from the furnace, reground and heated at 800 °C for 20 h. The final heating was generally at 1100 °C for 20 h, although for samples with high Co-concentration, temperatures up to 1250 °C were required to obtain single-phase products. Subsequent heat treatments were often employed to determine whether any changes in the phase(s) were obtained. Generally, samples were removed from the furnace at temperature and placed on a ceramic brick at the side of the furnace to cool. If it was thought necessary, samples were heated in a vertical tube furnace and quenched in liquid N_2 to avoid any phase changes associated with slow cooling.

It is assumed, for all samples, that oxidation of the Sb_2O_3 starting material occurred during reaction. All the phases encountered were solid solutions based on the known phases $ZnSb_2O_6$, $CoSb_2O_6$, $Zn_7Sb_2O_{12}$ and $Co_7Sb_2O_{12}$, all of which contain Sb(V). The ability to synthesise phase pure samples of $Zn_7Sb_2O_{12}$ and $Co_7Sb_2O_{12}$ at a temperature of 1225 °C with heating time of 2 h indicates that the Sb volatilisation is not a serious problem.

XRD was carried out with a Stoe Stadi P diffractometer, Mo$K\alpha_1$ radiation, using a small, linear position-sensitive detector. Powder neutron diffraction (ND) data were recorded on the POLARIS instrument at the Rutherford Appleton Laboratory. Rietveld refinement employed the graphical user interface (GUI) [19] for the DOS-based programme General Structure Analysis System (GSAS) [20].

3. Results and discussion

3.1. $Zn_{7-x}Co_xSb_2O_{12}$ solid solutions

Compositions with a general formula $Zn_{7-x}Co_xSb_2O_{12}$ were synthesised as outlined previously, with a final heating temperature of 1100 °C for 1–2 days. For composition $x = 0.5$, phase-pure β-polymorph was observed; composition $x = 1$ yielded a mixture of α- and β-polymorphs, while composition $x = 2$ yielded phase-pure α-polymorph. On reheating at 1250 °C, the composition $x = 1$ transformed into phase-pure α-polymorph. Composition $x = 2$ was unchanged upon heating at lower temperatures.

At high Co concentrations, $x = 6$ and 7, a small amount of the trirutile phase $Zn_{1-z}Co_zSb_2O_6$ was observed in the XRD pattern. Heating these samples at 1250 °C produced phase-pure α-polymorph; on reheating at 1100 °C, a small amount of $Zn_{1-z}Co_zSb_2O_6$ second phase was observed. Reheating phase-pure α-compositions $x = 4$ and 5 at 1000 °C also produced a small amount of trirutile phase.

From the results of heating samples at different temperatures and observing the reversibility of any changes, the pseudo-binary phase diagram, Fig. 1, was constructed. At high temperatures, the join is binary for all values of x. At lower temperatures, the join is binary only at lower values of x. The $\beta \rightarrow \alpha$ transition temperature decreases as cobalt is substituted for zinc, from 1225 ± 25 °C for the undoped end member [9]. No β phase was observed in the samples with $x \geqslant 2$.

Depending on composition and heat treatment conditions, a complete range of single-phase α solid solutions, $Zn_{7-x}Co_xSb_2O_{12}$, were obtained. A plot of cubic lattice parameter, a, vs. x in $Zn_{7-x}Co_xSb_2O_{12}$, Fig. 2, shows a negative deviation from the Vegard's law. This was not observed elsewhere in the literature; although Ilic et al. [14] present data over the whole series, no deviation from linearity was observed. However, errors in the measurements were not reported and the lattice parameter value of $Co_7Sb_2O_{12}$ was reported to be significantly greater than that measured here. The negative deviation in the lattice parameter plot [21,22], Fig. 2, is believed to be due to the octahedral site preference of Co^{2+}. Investigations into this are presented below.

At high x and lower temperatures, phase-pure α solid solutions were not obtained but instead, a small amount of trirutile secondary phase, of general formula $Zn_{1-z}Co_zSb_2O_6$, was present, as shown in Fig. 1. This means that the α solid solutions are Co-rich and Sb-deficient, compared with the general formula $Zn_{7-x}Co_xSb_2O_{12}$. Assuming that the cation:oxygen ratio remains at 3:4 in these Co-rich solid solutions, charge balance requires some oxidation of Co^{2+} to Co^{3+}, with the probable replacement mechanism

$$Sb^{5+} + 2Co^{2+} \rightarrow 3Co^{3+},$$

giving a general formula

$$Zn_{7-x}Co_{x+y}Sb_{2-y}O_{12}$$

or

$$Zn_{7-x}Co^{2+}{}_{x-2y}Co^{3+}{}_{3y}Sb_{2-y}O_{12}. \quad (1)$$

Since there are now two compositional variables, x and y, in the α solid solution, together with the possible compositional variable, z, in the trirutile solid solutions,

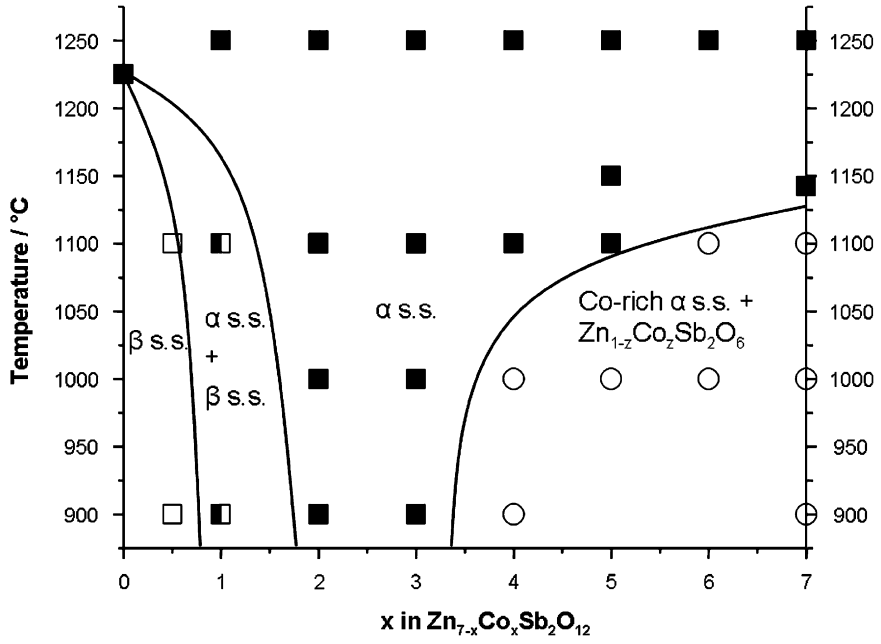

Fig. 1. Sub-solidus phase diagram for the pseudo-binary join represented by the general formula $Zn_{7-x}Co_xSb_2O_{12}$.

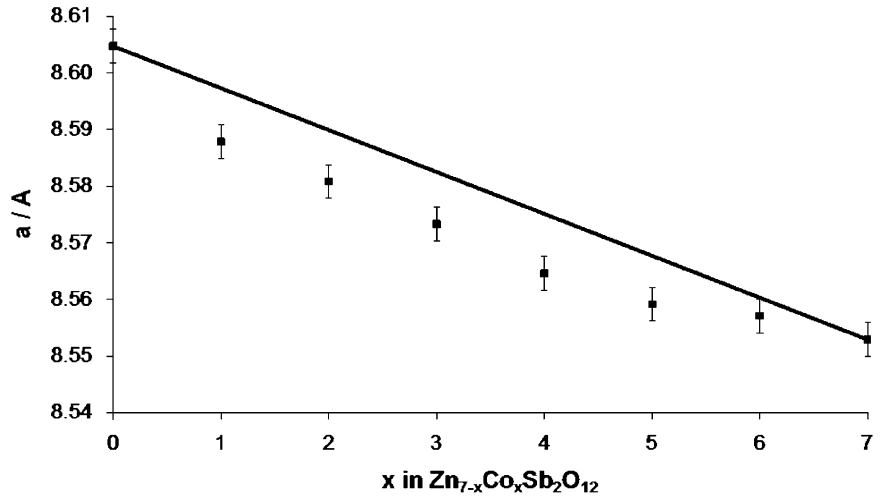

Fig. 2. Lattice parameter a vs. x for the α solid solutions, $Zn_{7-x}Co_xSb_2O_{12}$. The line between $x = 0$ and $x = 7$ is for comparison with the experimental data.

the compositions of the α and the trirutile phases in the two-phase region, Fig. 1, may vary both with overall composition, x, and temperature. Thus, the solvus curve limiting the T–x extent of the single-phase α solid solutions is as given in Fig. 1, but the composition(s) of the α phase within the two-phase region (α solid solution + trirutile solid solution) cannot be obtained from Fig. 1; determining this would require additional experimental studies. It was, however, noted that, for a given overall composition x, the lattice parameter of the α solid solution in the two-phase region was less than that in the single-phase samples quenched from higher temperature. This could be attributed to the presence of Co^{3+}, formula (1), for $y > 0$, leading to a decrease in the average Co–O bond length. Alternatively, it could be attributable (perhaps in part) to an increase in the value of x in the α solid solutions, depending on the Zn content, $1-z$, in the trirutile secondary phase.

3.2. Structural refinement of α-$Zn_{7-x}Co_xSb_2O_{12}$

Preliminary refinements using XRD data confirmed the exclusively octahedral coordination of Sb; in these refinements, the Co and Zn ions were both entered as Zn, making use of the insensitivity of X-rays to the elements of similar atomic number. A small amount of Sb was inserted to the tetrahedral site and its occupancy refined, returning a negative value. In subsequent refinements using ND data, the Sb was constrained to occupy only an octahedral site.

Neutron diffraction data for samples $x = 2$–5, quenched from 1250 °C, used to refine the structural model, taking the spinel structure as a starting point [9], to determine the occupancy of Zn and Co on the tetrahedral and octahedral sites. In the final refinements, Zn/Co occupancies on the tetrahedral and octahedral sites were refined independently without constraints as to the overall cation composition, but with the constraint that the spinel stoichiometry (AB_2O_4) was retained. Sb was placed exclusively on the octahedral sites, O was constrained to be fully occupied, since earlier refinements indicated full occupancy within experimental error. Free refinement of all parameters, apart from the occupancies of Sb and O, was allowed and a global minimum was achieved. The refined Co:Zn ratios, without applied constraints, were close to those of the expected sample compositions. A typical refinement plot, for $x = 4$, is presented in Fig. 3.

Refinement results are summarised in Table 1. Fig. 4 shows the tetrahedral site occupancy of Co as a function of composition, x. Also shown are two extremes of possible cation distribution. The dashed line represents a random mix of zinc and cobalt on each site and therefore, any site preference is more than offset by the increase in entropy associated with cation disorder. The solid line represents the case in which Co preferentially occupies the octahedral sites, but, for $x > 4$, also occupies the tetrahedral sites. In this case, the increased entropy associated with cation disorder is unable to offset the gain in enthalpy associated with cation order. In each of the samples investigated, less cobalt was found on the tetrahedral site than predicted if the distribution was purely random.

The octahedral preference of Co over Zn is attributed to crystal field effects. The d^7 Co(II) ion has a crystal field stabilisation energy of $\frac{4}{5}\Delta_O$ in a high-spin octahedral coordination, with a CFSE of $\frac{6}{5}\Delta_T$ in a tetrahedral coordination; the octahedral preference arises as $\Delta_T \approx \frac{4}{9}\Delta_O$. Since the closed shell d^{10} Zn(II) ion has no CFSE in either coordination, Co occupies preferentially an octahedral site, as was observed with Ni [8]. This preference, however, is not large; unlike Ni(II), which only occupied the octahedral sites, it is energetically acceptable for Co to exist in a tetrahedral coordination, as shown by the existence of $Co_7Sb_2O_{12}$. As a consequence, for intermediate values of x, the cation distribution is a compromise between the preference of Co for octahedral coordination and the high entropy associated with random cation site occupancy. In the Ni-doped system, by contrast, the octahedral preference of Ni is so large that the increased entropy term at higher temperatures is not sufficient to induce any mixing [8].

This non-random cation distribution provides an explanation for the deviation from Vegard's law (Fig. 2). A random occupation by the two cations over tetrahedral and octahedral sites would result in the solid line between the end members in Fig. 2. In practice the experimental lattice parameters and cell volumes are smaller than expected from Vegard's law indicating a greater lattice stabilisation and lattice energy associated with the preference of a more ordered cation distribution.

It should be noted that the degree of cation disorder may be somewhat sample-specific and dependent on synthesis method and temperature. Samples synthesised by sol–gel methods, for example samples produced by Lisboa-Filho et al. [23], who used a final firing temperature of 1000 °C for 1 h, may have less mixing due to the reduced contribution of the entropy term, $T\Delta S$, to the Gibb's free energy. If the degree of cation order could be varied for a given x, this may be indicated by a variation in lattice parameter.

3.3. The ternary phase diagram ZnO–Sb_2O_5–CoO

The sub-solidus compatibility relations in the ternary system ZnO–Sb_2O_5–CoO were determined following the heat treatment experiments on 26 compositions, Table 2.

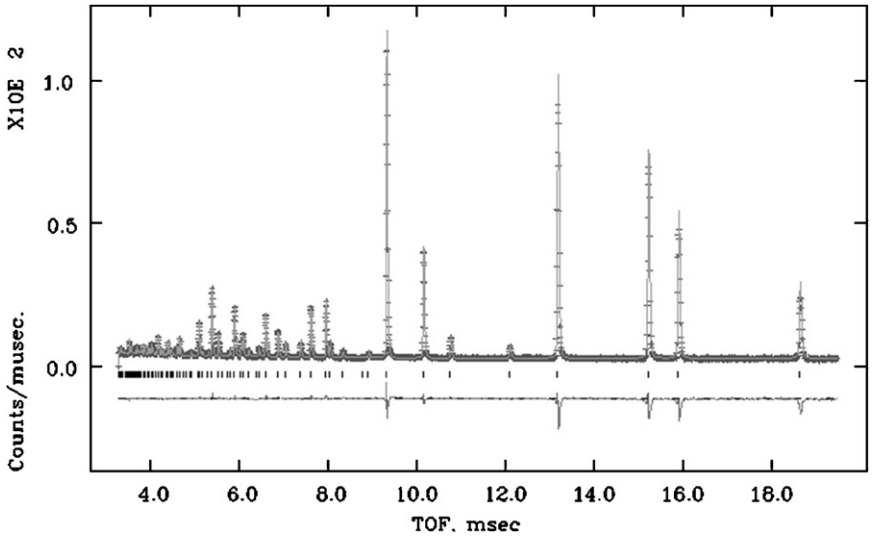

Fig. 3. Observed, calculated and difference fits from neutron data for the composition $Zn_3Co_4Sb_2O_{12}$.

Table 1
Refined parameters for samples $x = 2$–5 in $Zn_{7-x}Co_xSb_2O_{12}$; values for the end members are taken from the literature

X	0 [9]	2	3	4	5	7 [14]
a/Å	8.6047	8.58083 (3)	8.57326 (4)	8.56459 (3)	8.55917 (9)	8.5371 (3)
Oxygen coordinate	0.2591 (8)	0.259559 (24)	0.259642 (1)	0.259721 (24)	0.259778 (5)	Not available
d_{oct-O}/Å	2.072 (5)	2.06644 (19)	2.06397 (1)	2.06126 (19)	2.05950 (2)	2.051 (3)
d_{tet-O}/Å	2.015 (8)	1.9999 (4)	1.99934 (1)	1.99849 (35)	1.99807 (2)	1.942 (3)
$100*U_{oct}$/Å^2	1.33 (6)	0.848 (18)	0.767 (11)	0.668 (20)	0.583 (11)	0.64 (3)
$100*U_{tet}$/Å^2	1.29 (10)	0.822 (20)	0.810 (12)	0.753 (23)	0.751 (14)	0.17 (5)
$100*U_O$/Å^2	1.64 (22)	0.850 (9)	0.825 (6)	0.770 (9)	0.767 (6)	0.3 (1)
Co on tet	0	0.06 (3)	0.23 (2)	0.58 (3)	1.19 (3)	3
Co on oct	0	1.95 (4)	2.75 (3)	3.41 (4)	3.82 (2)	4
χ^2	4.17	5.01	4.56	4.70	3.93	Not available
wR_p	6.76	3.59	3.42	3.59	5.70	14.40
R_p	8.23	5.70	5.72	5.70	5.46	10.08

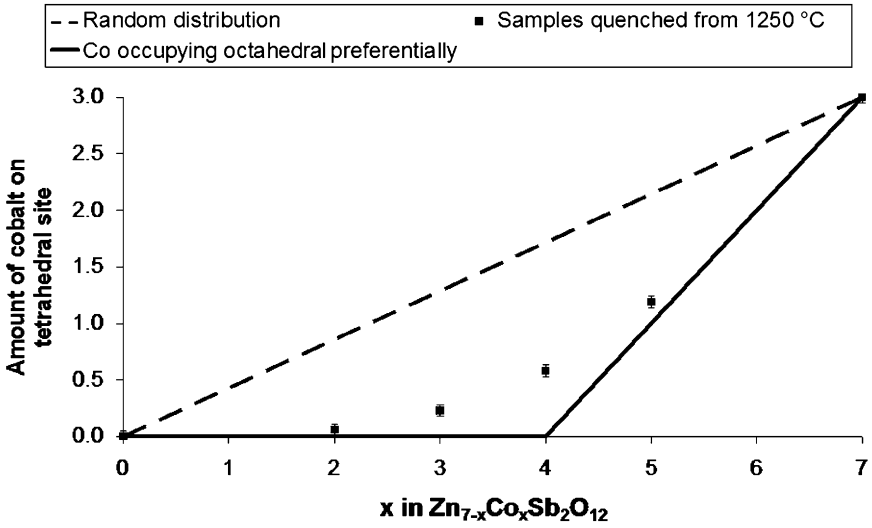

Fig. 4. Concentration of cobalt ions adopting a tetrahedral geometry. The dashed line represents a random distribution of Zn and Co ions over the tetrahedral sites and those octahedral sites not occupied by Sb. The solid line represents octahedral site preference for Co and the squares are the experimental data.

All samples were given a final heat treatment of 1100 °C, as lower temperatures often did not yield complete reaction. Generally, heating at 1100 °C for 20 h was sufficient to ensure complete reaction, but reaction times of 40 h were often necessary before it was confidently felt that equilibrium had been achieved.

The ternary phase diagram, constructed from the data in Table 2, is presented in Fig. 5. The phase diagram contains five solid–solution regions: first, there is a full solid–solution range between the trirutile phases $ZnSb_2O_6$ and $CoSb_2O_6$. The two phases have very similar lattice parameters; the peak shift between the two end members is minimal. Second, at low x, a small amount of Co can substitute into β-$Zn_7Sb_2O_{12}$. Third, for $x \geqslant 2$, a large range of solid solutions exist between α-$Zn_7Sb_2O_{12}$ and $Co_7Sb_2O_{12}$. At higher cobalt concentrations, the solid solutions are non-stoichiometric as a small amount of Co^{3+} substitutes for Sb^{5+}/Co^{2+}.

Fourth, ZnO dissolves in CoO up to 35%, while, fifth, a significant amount of CoO, 20%, dissolves in ZnO, both consistent with previous literature reports [24]. The remainder of the phase diagram is divided into two-phase and three-phase compatibility regions. No attempt was made to study the compositions containing $>50\%$ Sb_2O_5.

4. Conclusions

A complete solid–solution range between α-$Zn_7Sb_2O_{12}$ and $Co_7Sb_2O_{12}$ forms at 1250 °C. Substitution of Co for Zn decreases the $\beta \rightarrow \alpha$ phase transition temperature; at compositions $x \geqslant 2$, no β-polymorph is observed at any temperature. When α-$Zn_{7-x}Co_xSb_2O_{12}$ solid solutions with high x are reheated at lower temperatures, a small amount of the antimony-rich phase $Zn_{1-z}Co_zSb_2O_6$ is observed and the α solid solutions become Co-rich and Sb-deficient; a decrease in the lattice parameter of the spinel phase occurs, attributed to the partial oxidation of Co^{2+} to Co^{3+}.

Rietveld refinement using ND data shows Co to be substituted for Zn on both octahedral and tetrahedral sites of the α solid solutions. The octahedral site preference of

Table 2
Phases present at different compositions of ZnO, CoO and Sb_2O_5

%ZnO:%CoO:%Sb_2O_5	Phase(s) present at 1100 °C	Time heated at 1100 °C/h
38:12:50	ZC-ss	20
25:25:50	ZC-ss	20
12:38:50	ZC-ss	20
70:5:25	α-ss + β-ss + ZC-ss	20
50:20:30	α-ss + ZC-ss	20
34:33:33	α-ss + ZC-ss	20
15:55:30	α-ss + ZC-ss	20
81:6:13	β-ss	40
76:12:12	α-ss + β-ss	40
63:25:12	α-ss	40
50:38:12	α-ss	40
38:50:12	α-ss	20
25:63:12	α-ss	20
13:75:12	Co-rich α + ZC-ss	20
0:88:12	Co-rich α + ZC-ss	40
90:5:5	β-ss + ZnO-ss	40
80:14:6	α-ss + β-ss + ZnO-ss	40
50:45:5	α-ss + ZnO-ss + CoO-ss	20
14:80:6	α-ss + CoO-ss	40
5:87:8	Co-rich α + CoO-ss	20
0:91:9	Co-rich α + CoO	20
0:95:5	Co-rich α + CoO	20
80:20:0	ZnO-ss + Co-ss	20
60:40:0	ZnO-ss + CoO-ss	20
40:60:0	ZnO-ss + CoO-ss	40
20:80:0	CoO-ss	40

Key: α-ss = α-$Zn_{7-x}Co_xSb_2O_{12}$, β-ss = β-$Zn_{7-x}Co_xSb_2O_{12}$, ZC-ss = $Zn_{1-z}Co_zSb_2O_6$, Co-ss = $Co_{1-x}Zn_xO$, Zn-ss = $Zn_{1-x}Co_xO$.

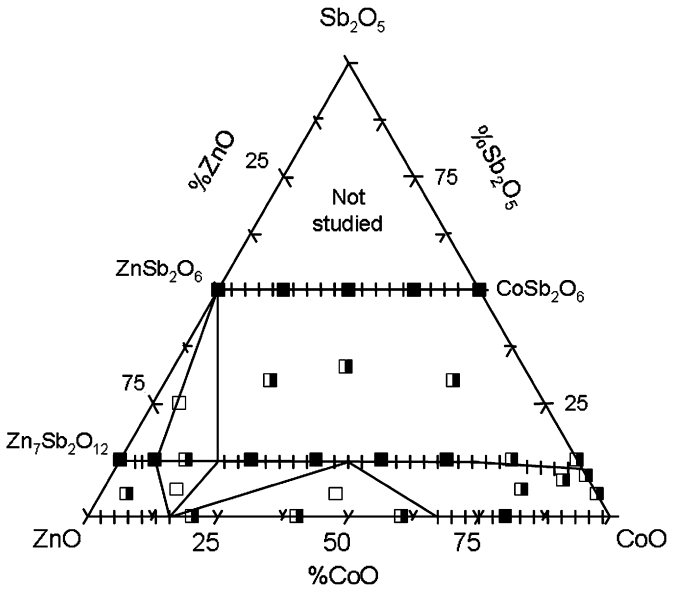

Fig. 5. Sub-solidus compatibility relations at 1100 °C for the ZnO–Sb_2O_5–CoO system. Closed, half-closed and open squares refer, respectively, to 1-, 2- and 3-phase products.

Co means that it is favourable for Co to occupy the octahedral sites up to $x = 4$ and the tetrahedral sites thereafter. Since this preference is small, relative to that of Ni, the entropy contribution to the Gibb's free energy at the high-synthesis temperatures means that a small amount of tetrahedral occupation occurs. This partial mixing of Co and Zn on the tetrahedral and octahedral sites causes the lattice parameter plot to deviate from linearity, the octahedral preference of Co causing the negative deviation.

Acknowledgments

We thank Dr. R.I. Smith for assistance with the POLARIS instrument and EPSRC for the financial support.

References

[1] S. Ezhilvalavan, T.R.N. Kutty, Appl. Phys. Lett. 68 (1996) 2693–2695.
[2] M.A.L. Nobre, S. Lanfredi, Appl. Phys. Lett. 81 (2002) 451–453.
[3] M.A.L. Nobre, S. Lanfredi, Mater. Lett. 50 (2001) 322–327.
[4] D.R. Clarke, J. Am. Ceram. Soc. 82 (1999) 485–502.
[5] M. Inada, Jpn. J. Appl. Phys. 18 (1979) 1439–1446.
[6] C.H. Lu, N. Chyi, H.W. Wong, W.J. Hwang, Mater. Chem. Phys. 62 (2000) 164–168.
[7] S.G. Cho, H. Lee, H.S. Kim, J. Mater. Sci. 32 (1997) 4283–4287.
[8] R. Harrington, G.C. Miles, A.R. West, J. Eur. Ceram. Soc. 26 (2006) 2307–2311.
[9] G.C. Miles, A.R. West, J. Am. Ceram. Soc. 88 (2005) 396–398.
[10] G.C. Miles, C.A. Kirk, R. Harrington, A.R. West, Solid State Sci., submitted for publication.
[11] T.K. Gupta, J. Am. Ceram. Soc. 73 (1990) 1817–1840.
[12] M. Inada, Jpn. J. Appl. Phys. 19 (1980) 409–419.
[13] D. Poleti, D. Vasovic, L. Karanovic, Z. Brankovic, J. Solid State Chem. 112 (1994) 39–44.
[14] A. Ilic, B. Antic, D. Poleti, D. Rodic, I. Petrovic-Prelevic, L.J. Karanovic, J. Phys.-Condens. Matter 8 (1996) 2317–2325.
[15] M.S.L. Brito, M.T. Escote, C.O.P. Santos, P.N. Lisboa-Filho, E.R. Leite, J.B.L. Oliveira, L. Gama, E. Longo, Mater. Chem. Phys. 88 (2004) 404–409.
[16] D.S. Gouveia, A.G. Souza, M. de Maurera, C.E.F. da Costa, I.M.G. Santos, S. Prasad, J.B. de Lima, C.A. Paskocimas, E. Longo, J. Therm. Anal. 67 (2002) 459–464.
[17] D.S. Gouveia, R. Rosenhaim, M.A.M.A. de Maurera, S.J.G. Lima, C.A. Paskocimas, E. Longo, A.G. Souza, I.M.G. Santos, J. Therm. Anal. Calorim. 75 (2004) 453–460.
[18] K. Krezhov, P. Konstantinov, J. Phys.-Condens. Matter 5 (1993) 9287–9294.
[19] B.H. Toby, J. Appl. Crystallogr. 34 (2001) 210–213.
[20] A.C. Larson, R.B. Von Dreele, General Structural Analysis System. Los Alamos National Laboratory, Report LAUR 86-748, 2000.
[21] M. Castellanos, A.R. West, J. Mater. Sci. 14 (1979) 450–454.
[22] M. Castellanos, A.R. West, J. Chem. Soc. Faraday Trans. I 76 (1980) 2159–2169.
[23] P.N. Lisboa, C. Vila, M.S. Goes, C. Morilla-Santos, L. Gama, E. Longo, W.H. Schreiner, C.O. Paiva-Santos, Mater. Chem. Phys. 85 (2004) 377–382.
[24] J. Robin, Ann. Chim. (Paris) 47 (1955) 830.